RESEARCH ARTICLE

Figures and figure supplements

Structure and function of the ROR2 cysteine-rich domain in vertebrate noncanonical WNT5A signaling

Samuel C Griffiths and Jia Tan *et al*.

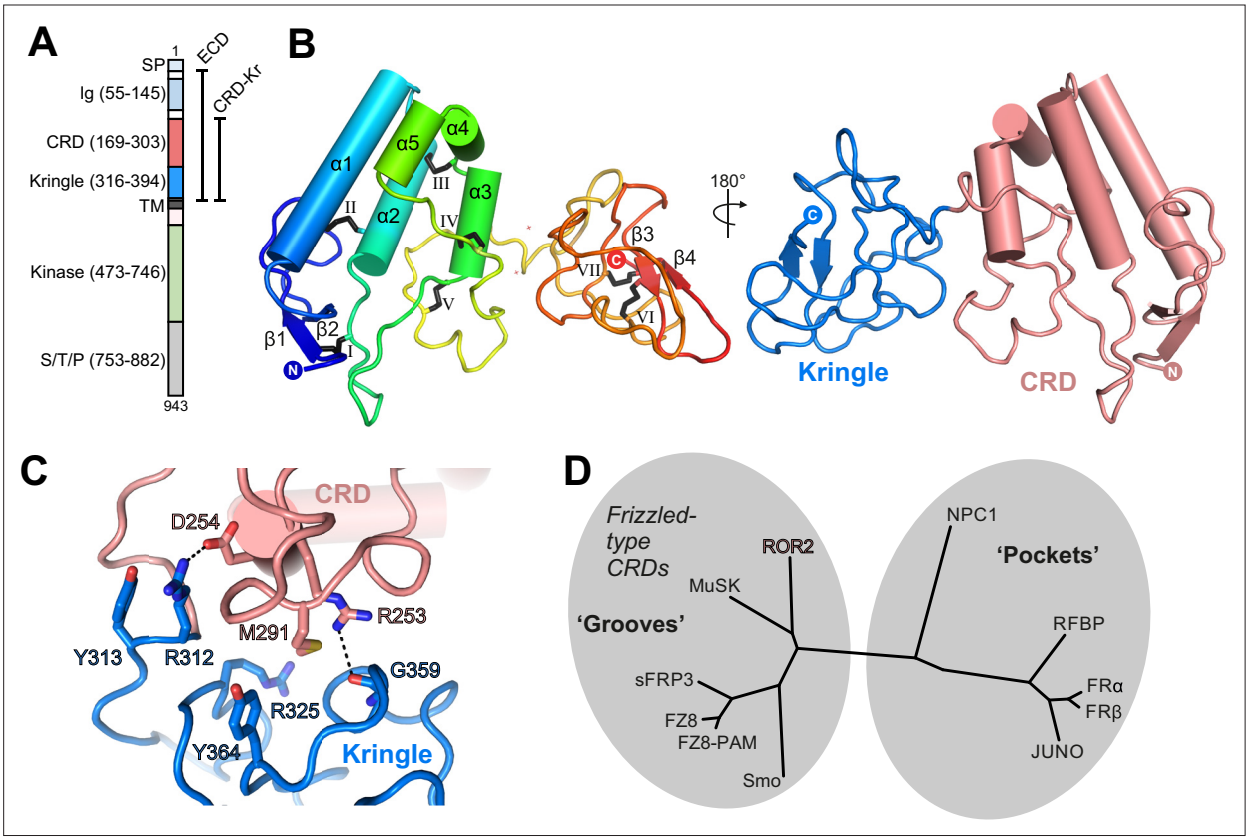

Figure 1. Structure of the ROR2 cysteine-rich domain (CRD) and Kringle (Kr) domains. (**A**) Domain layout of ROR2 and constructs used in this study. SP, signal peptide; S/T/P, serine/threonine/proline-rich domain. Other domains are defined in the text. (**B**) Cartoon representation of the ROR2 CRD-Kr structural unit colored in a rainbow representation (N terminus: blue, C terminus: red), with secondary structural elements indicated and disulfide bonds numbered using Roman numerals. The right panel shows a two-domain representation of ROR2, with the CRD in salmon and the Kr domain in blue. (**C**) Close-up view on the ROR2 CRD-Kr interface rotated 90° relative to (**B**). Interface residues are shown in stick representation and color-coded as in B, right panel. Hydrogen bonds are displayed as a dashed line. (**D**) Structural phylogenetic analysis of CRDs, adapted from Figure 5 of ***Nachtergaele et al., 2013***, to include ROR2.

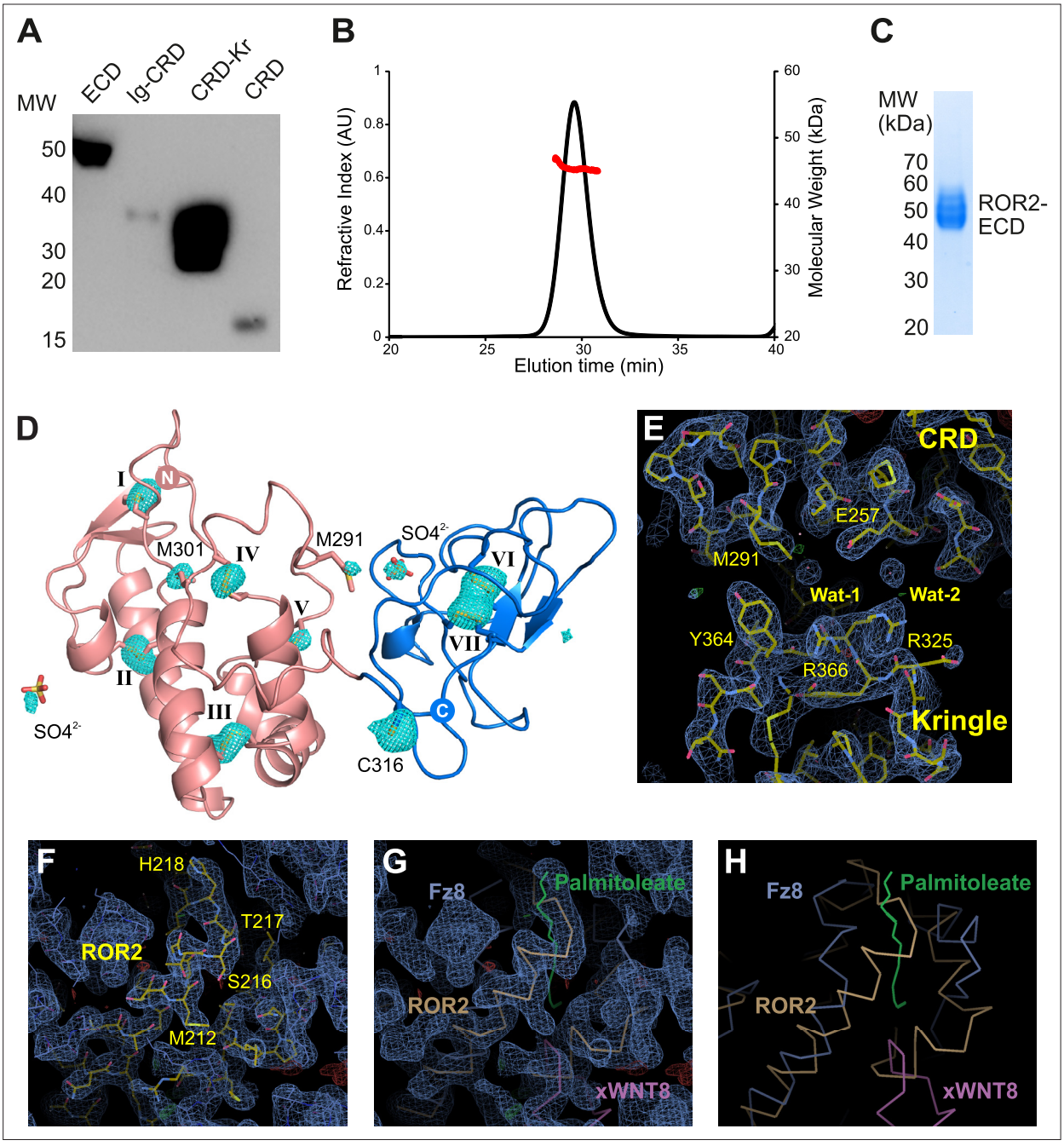

Figure 1—figure supplement 1. ROR2 purification, characterization, and structure solution. (**A**) Western blot analysis of the secretion of soluble ROR2 constructs from HEK293T cells. Deletion of the Kringle (Kr) domain impairs secretion. (**B**) Size exclusion chromatography-multiangle light scattering (SEC-MALS) analysis of the ROR2 extracellular region (ECD) at 2 mg/ml (48 μM). The ROR2 ECD elutes as a monomeric species with a molecular weight of 45.4 kDa, as displayed by the red line. (**C**) Purity assessment by SDS-PAGE of ROR2 ECD construct purified via IMAC and SEC. (**D**) Identification of sulfur sites in ROR2 CRD-Kr using long-wavelength data collection at I23. A total of eight disulfide bonds (I–VII) could be resolved, as well as four methionine and one cysteine side chains, as well as two sulfate ions. (**E–H**) Structure solution of ROR2 CRD-Kr using MR-SAD. The final structure refined using *PHENIX* and corresponding sigma-A weighted $2F_o$-map at 1σ (blue) and F_o-F_c density at ±3.5σ (green/red) are shown. (**E**) Focuses on the ROR2 CRD-Kr interface, whereas (**F–H**) are centered around the palmitoleate binding site commonly conserved in Frizzled (FZ)-type CRDs. This site is occluded in the ROR2 structure by a rearrangement of a loop (M212-T219) that overlaps with palmitoleate binding, observed, for example, in the FZ8-xWNT8 complex structure (PDB ID: 4F0A) (***Janda et al., 2012***). The superposition of ROR2 and the FZ8xWNT8 complex (**G**) and (**H**) illustrates this rearrangement.

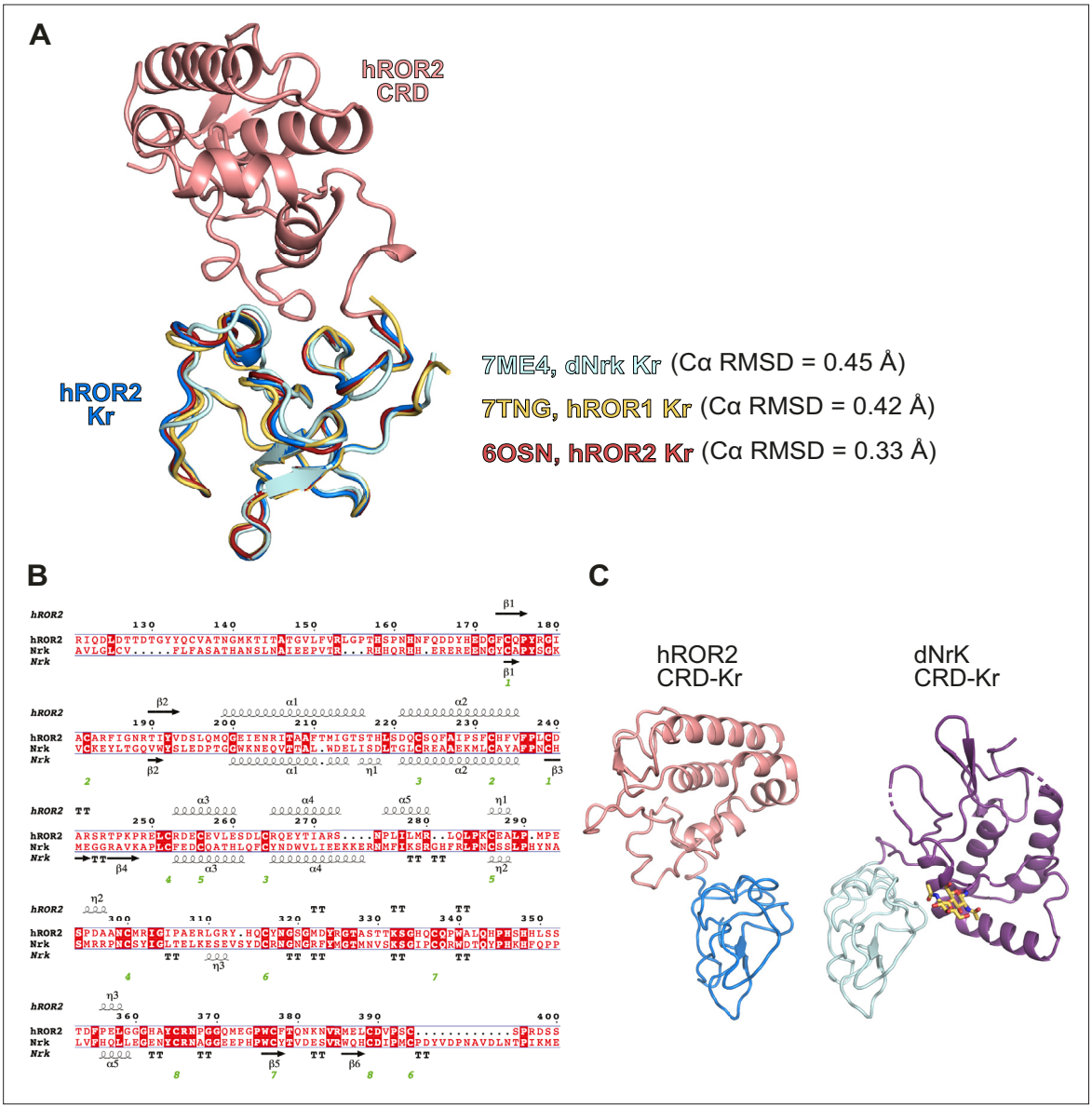

Figure 1—figure supplement 2. Comparison of the ROR2 Kringle (Kr) to other related Kr structures. (**A**) Structural superposition of the ROR2 cysteine-rich domain (CRD)-Kr (CRD, salmon; Kr, blue) with described human ROR1 Kr (yellow, PDB 7TNG), human ROR2 Kr (red, PDB 6OSN), and *Drosophila* Nrk (light turquoise, PDB 7ME4). Cα root mean square deviations (RMSDs) shown are with respect to ROR2 Kr within the CRD-Kr structure. (**B**) Sequence alignment of the human ROR2 and *Drosophila* Nrk CRD-Kr tandem domains. (**C**) Comparison of the human ROR2 and *Drosophila* Nrk CRD-Kr tandem domains shown as ribbon representation. The CRDs of ROR2 and Nrk are shown in the same spatial orientation.

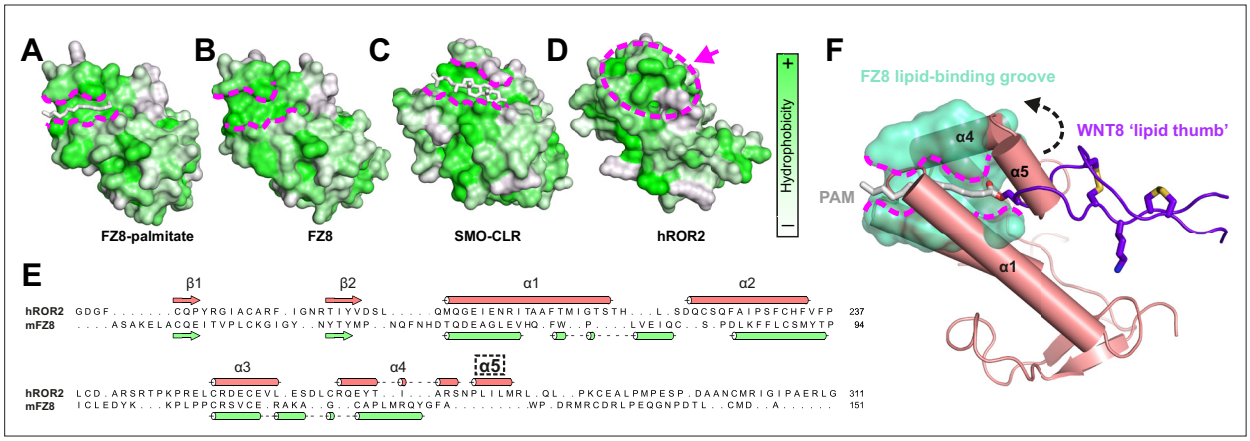

Figure 2. Comparison of the ROR2 cysteine-rich domain (CRD) to other Frizzled (FZ)-type CRDs. (**A–D**) CRDs are shown as surface representation and colored according to hydrophobicity (green: hydrophobic to white: hydrophilic). Displayed structures: (**A**) FZ8-PAM (palmitoleate) complex (PDB 4F0A) (***Janda et al., 2012***), (**B**) FZ8-apo (PDB 1IJY) (***Dann et al., 2001***), (**C**) Smoothened-CLR (cholesterol) complex (PDB 5L7D) (***Byrne et al., 2016***), and (**D**) ROR2 (from this study). (**E**) Structure-based sequence alignment of the ROR2 and FZ8 CRDs. The ROR2 inserted helix α5 is shown with a dashed box. (**F**) Structural superposition of the ROR2 CRD (salmon) with the FZ8-WNT8 (green/purple, PDB 4F0A) complex. Only the WNT8 'lipid thumb' is shown, with the covalently attached palmitoleate modification in white.

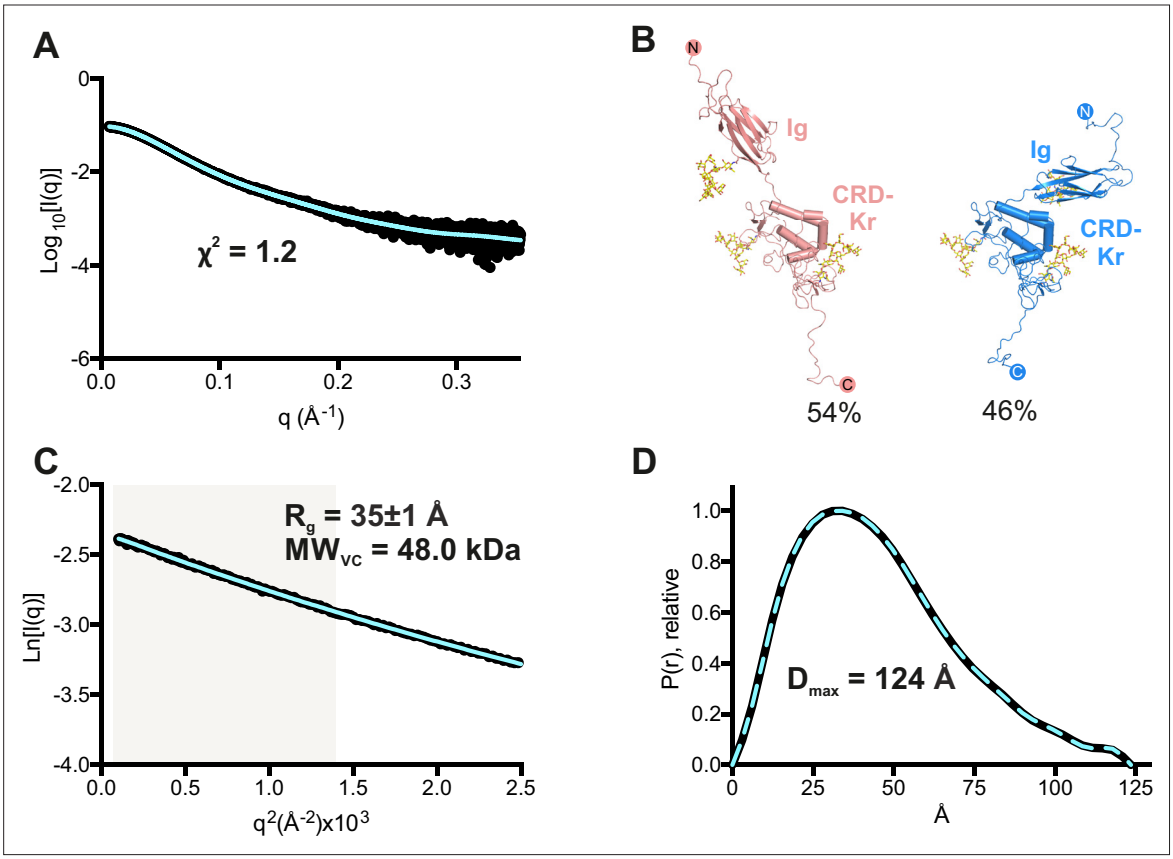

Figure 2—figure supplement 1. Small-angle X-ray scattering (SAXS) solution structure of the ROR2 extracellular region (ECD). (**A**) Experimental scattering curve (black) and calculated scattering from models (blue), shown to a maximum momentum transfer of 0.35 Å^{-1}. A fitting residual between the experimental and calculated scattering patterns is displayed. (**B**) The ROR2 ECD data is best explained using two major models in the given populations as calculated by Multi-FOXS, indicating flexibility in the linker between the immunoglobulin (Ig) and the CRD-Kr regions. (**C**) Experimental (black) and calculated (blue) Guinier region. The shaded area indicates the region used for R_g analysis. The calculated radius of gyration (R_g) and molecular weight derived from the volume of correlation metric V_c (MW_{VC}) are displayed. (**D**) Normalized pair distance distribution (P(r)) function and derived maximum intra-particle distance distribution function (D_{max}). CRD, cysteine-rich domain; Kr, Kringle.

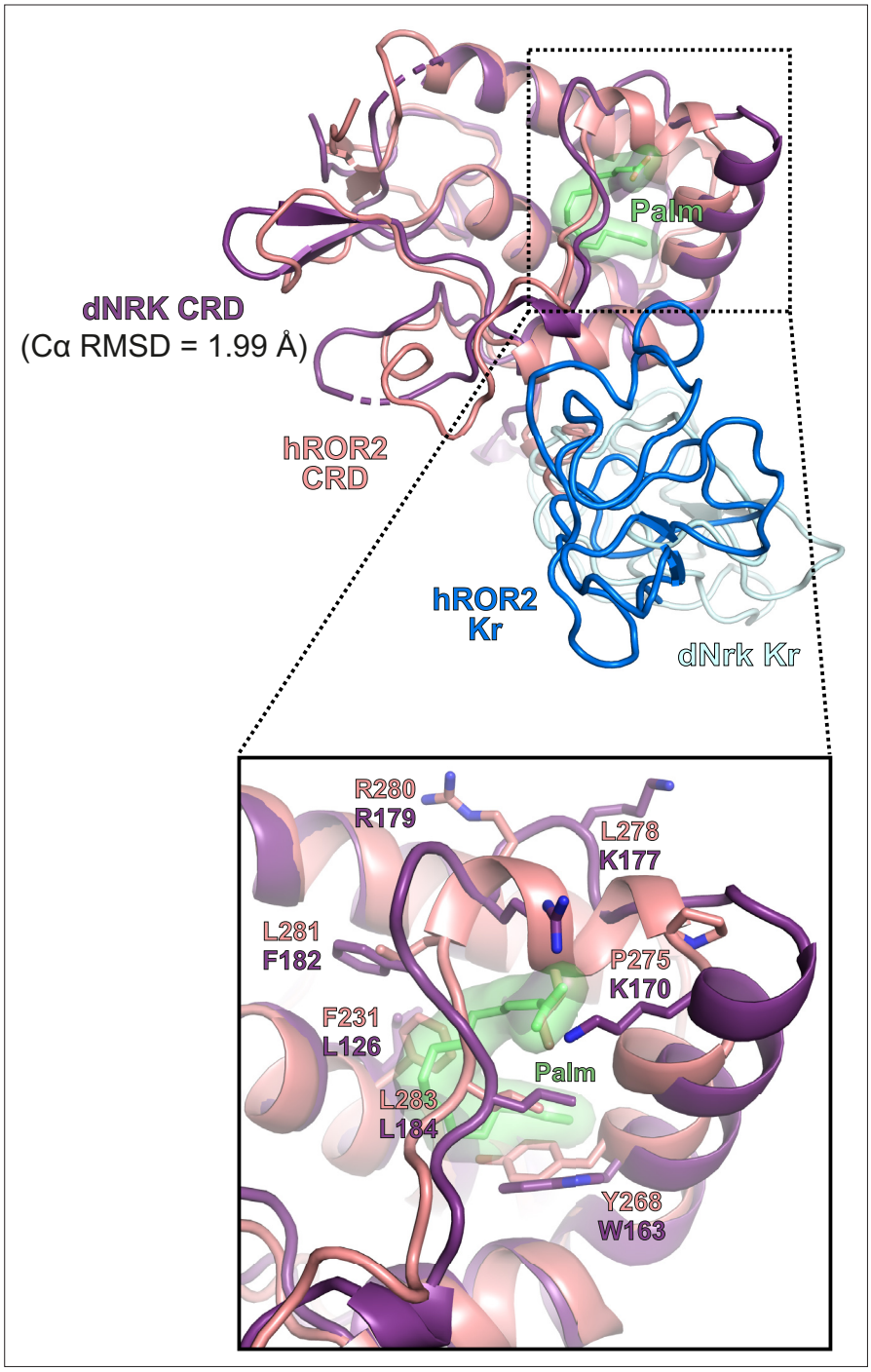

Figure 2—figure supplement 2. Comparison of the human ROR2 and *Drosophila* Nrk cysteine-rich domains (CRDs). Structural superposition of the human ROR2 CRD (salmon) with the *Drosophila* Nrk CRD (purple, PDB 7ME4). The Cα root mean square deviation (RMSD) between the two structures is shown. The close-up view shows the region surrounding the internally buried fatty acid in the *Drosophila* Nrk CRD.

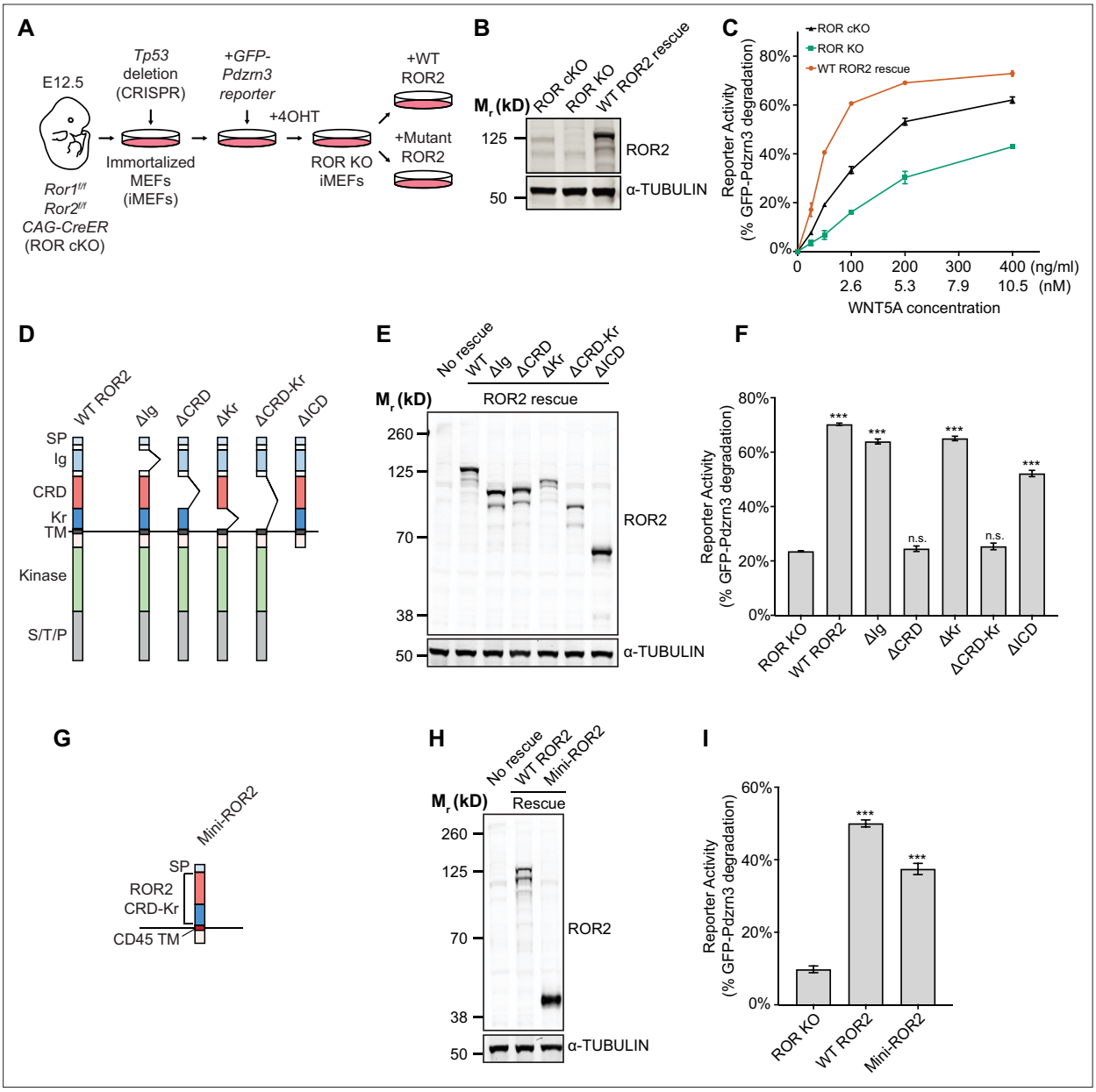

Figure 3. Requirement of the ROR2 cysteine-rich domain (CRD) in WNT5A signaling. (**A**) Workflow of the ROR2 central rescue paradigm. Primary mouse embryonic fibroblasts (MEFs) generated from E12.5 *Ror1*$^{f/f}$*; Ror2*$^{f/f}$*; CAG-CreER* conditional knockout (ROR cKO) mouse embryos were immortalized by CRISPR/Cas9-mediated deletion of the *Tp53* gene. A WNT5A-ROR signaling reporter (GFP-Pdzrn3) was stably inserted in the immortalized MEFs (iMEFs) via piggyBac-based transposition. ROR cKO iMEFs were then treated with 4-hydroxytamoxifen (4OHT) to activate the CreER recombinase to delete the *Ror1* and *Ror2* genes, resulting in ROR knockout (ROR KO) iMEFs (genotype: *Ror1*$^{-/-}$*; Ror2*$^{-/-}$*; CAG-CreER*). To compare the function of ROR2 domain truncation mutants, wildtype (WT) or mutant ROR2 rescue constructs were re-expressed in ROR KO iMEFs via lentiviral transduction. (**B**) Western blot showing the expression of endogenous ROR2 (the 125kD band) in ROR cKO iMEFs, the loss of ROR2 expression in ROR KO iMEFs, and re-expression of the WT ROR2 rescue construct (Flag-tagged). (**C**) Dose-response curves showing WNT5A-ROR signaling activity, assayed by GFP-Pdzrn3 degradation, as a function of WNT5A concentration in ROR cKO iMEFs, ROR KO iMEFs, or ROR KO iMEFs expressing the WT ROR2 rescue construct. All iMEFs were pretreated with Wnt-C59, an inhibitor of the membrane-bound *O*-acyltransferase Porcupine (***Proffitt et al., 2013***), to block the activity of endogenous WNTs. Each data point was calculated from the median fluorescence ([before WNT5A stimulation – after WNT5A stimulation]/before WNT5A stimulation) of the GFP-Pdzrn3 reporter from 10,000 cells. Error bars represent ± SEM calculated from two technical replicates (two independent WNT5A stimulation experiments of the same cell lines). (**D**) Schematic of ROR2 domain truncation mutants. (**E**) Western blot showing the expression of the WT and mutant ROR2 constructs. ROR2 protein variants were detected using a rabbit polyclonal anti-ROR2 antibody. α-TUBULIN was used as the loading control. (**F**) Quantification of the effects of ROR2 mutant variants in rescuing WNT5A-ROR signaling, as assayed by GFP-Pdzrn3 degradation. Cells were treated with 200 ng/ml (5.3 nM) WNT5A for 6 hr. Error bars represent ± SEM calculated from three technical replicates. t-Test (unpaired) was performed to determine statistical significance of each rescue construct vs. the no rescue control (ROR KO cells). (**G**) Schematic of the mini-ROR2

Figure 3 continued on next page

Figure 3 continued

construct. (**H**) Anti-ROR2 western blot showing the expression of the WT ROR2 and mini-ROR2 rescue constructs. α-TUBULIN was used as the loading control. (**I**) Quantification of the effect of mini-ROR2 in rescuing WNT5A-ROR signaling, as assayed by GFP-Pdzrn3 degradation. Cells were treated with 200 ng/ml (5.3 nM) WNT5A for 6 hr. Error bars represent ± SEM calculated from three technical replicates. t-Test (unpaired) was performed to determine statistical significance of each rescue construct vs. the no rescue control (ROR KO cells). ***Figure 3—source data 1*** (related to panel C). ***Figure 3—source data 2*** (related to panel F). ***Figure 3—source data 3*** (related to panel I).

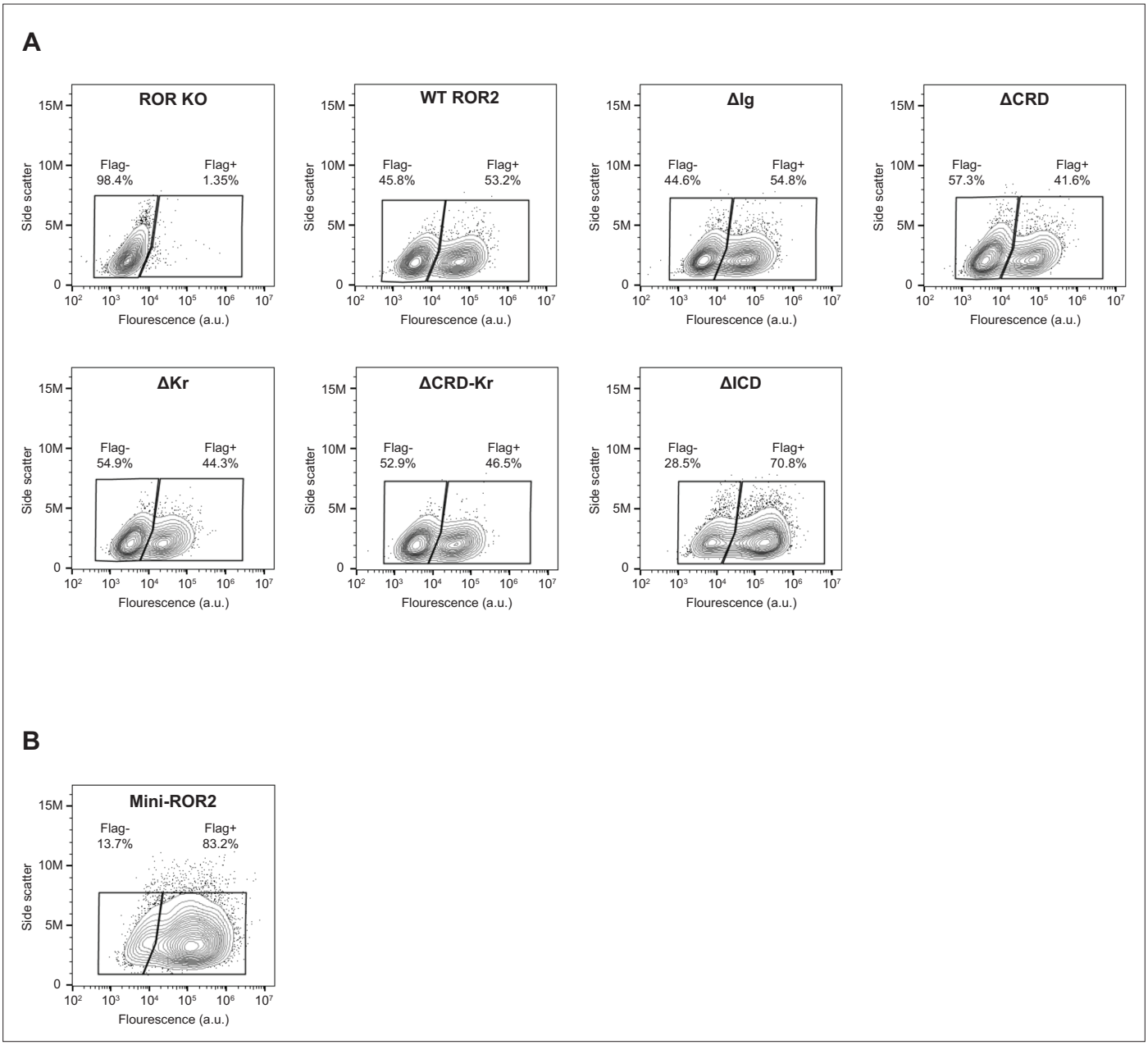

Figure 3—figure supplement 1. Surface expression analysis of ROR2 domain truncation mutants and mini-ROR2. Wildtype (WT) and ROR2 domain truncation mutants were tagged on the N-terminus with a Flag tag (see Methods for details). Anti-Flag immunostaining was performed on live cells to assess the cell surface expression levels of ROR2 domain truncation mutants (**A**) and mini-ROR2 (**B**). ROR knockout (KO) cells and ROR KO cells expressing the WT ROR2 rescue construct were used as the negative and positive controls, respectively.

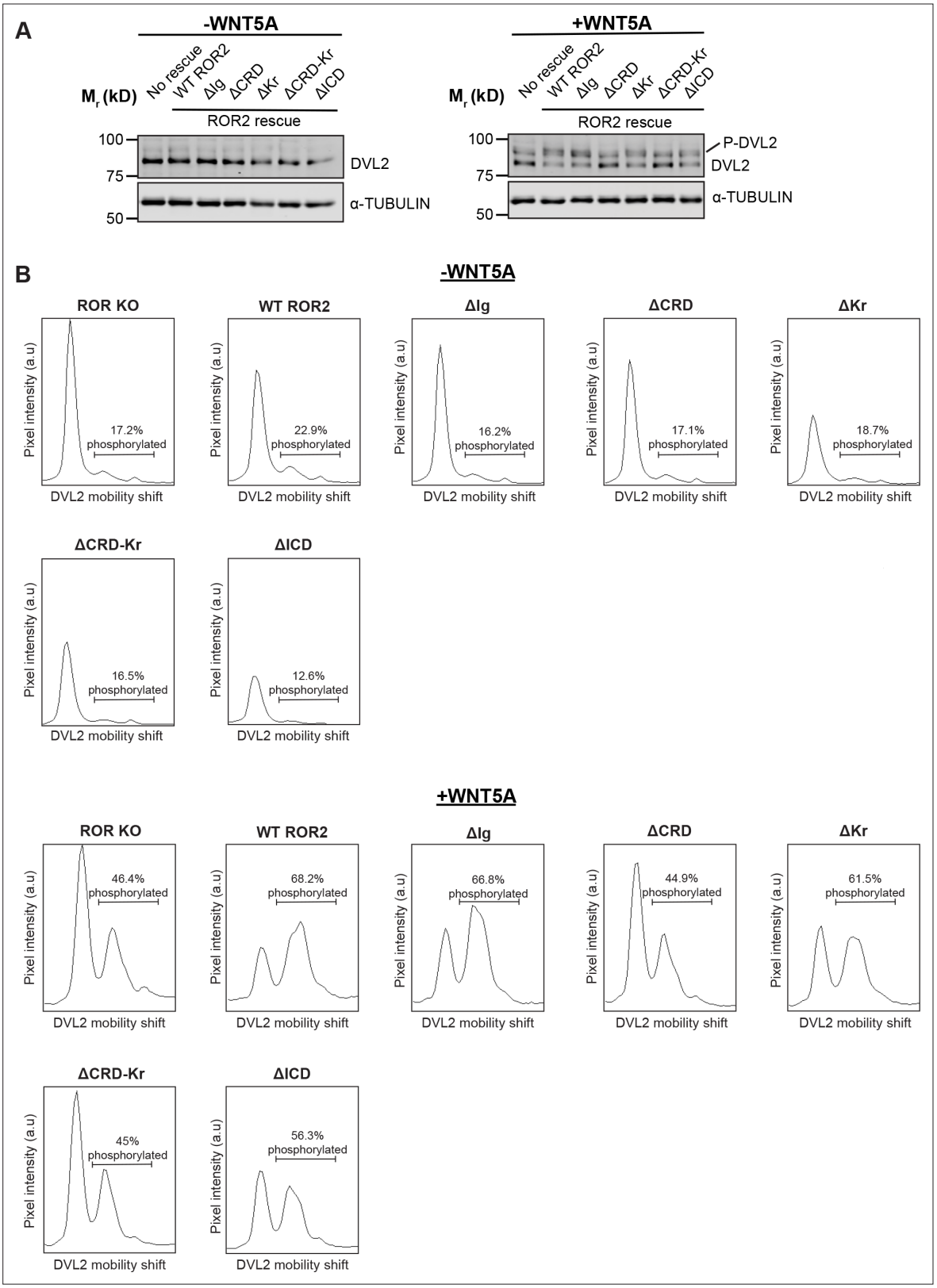

Figure 3—figure supplement 2. Requirement of the ROR2 cysteine-rich domain (CRD) in WNT5A signaling, as assayed by Dishevelled 2 (DVL2) phosphorylation. (**A**) Western blots showing the extents of DVL2 phosphorylation in ROR knockout (KO) immortalized mouse embryonic fibroblasts (iMEFs) and in ROR KO iMEFs expressing wildtype (WT) or domain truncation mutants of ROR2, before and after WNT5A stimulation (100 ng/ml or 2.6 nM WNT5A for 6 hr). DVL2 phosphorylation causes a delay in the gel mobility DVL2 in SDS-PAGE, which can be visualized as an upward shift of the

Figure 3—figure supplement 2 continued on next page

Figure 3—figure supplement 2 continued

DVL2 band (marked as P-DVL2). (**B**) Quantification of DVL2 phosphorylation by densitometry. % phosphorylation is calculated as the portion of total DVL2 signal that is upshifted.

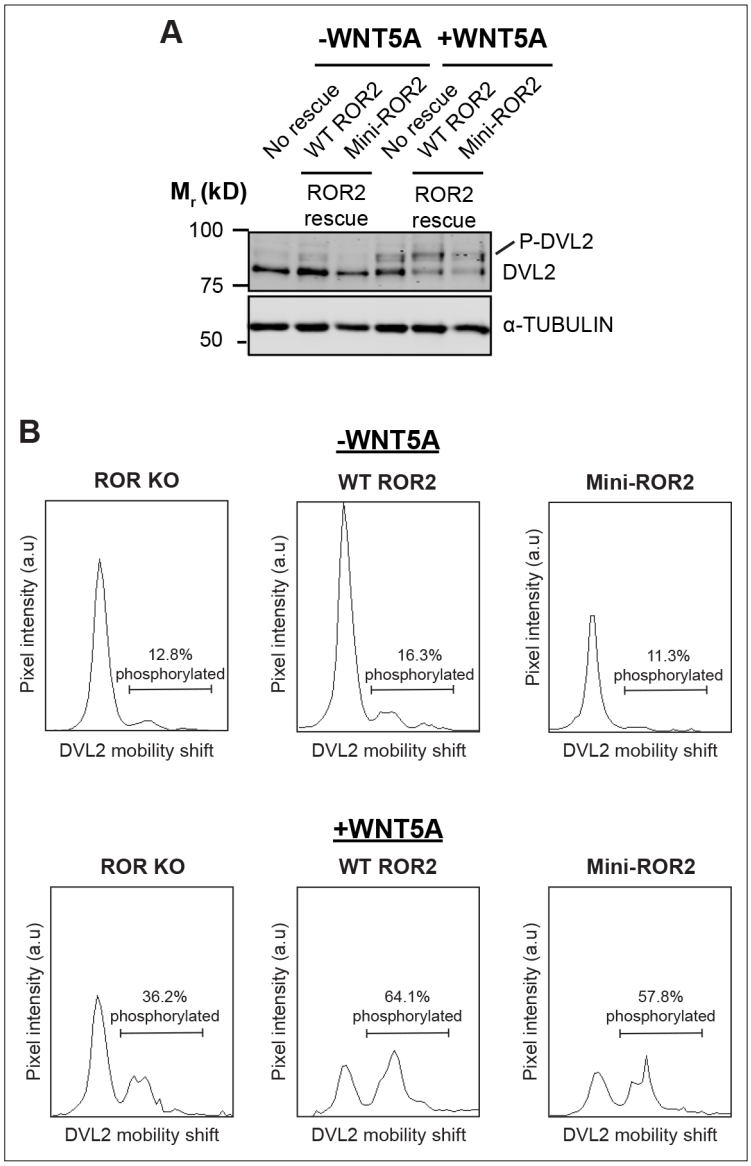

Figure 3—figure supplement 3. The ability of mini-ROR2 to rescue WNT5A signaling, as assayed by Dishevelled 2 (DVL2) phosphorylation. (**A**) Western blots showing the extents of DVL2 phosphorylation in ROR KO iMEFs and in ROR KO iMEFs expressing WT ROR2 or mini-ROR2, before and after WNT5A stimulation (100ng/ml or 2.6nM WNT5A for 6hr). (**B**) Quantification of DVL2 phosphorylation by densitometry. % phosphorylation is calculated as the portion of total DVL2 signal that is upshifted.

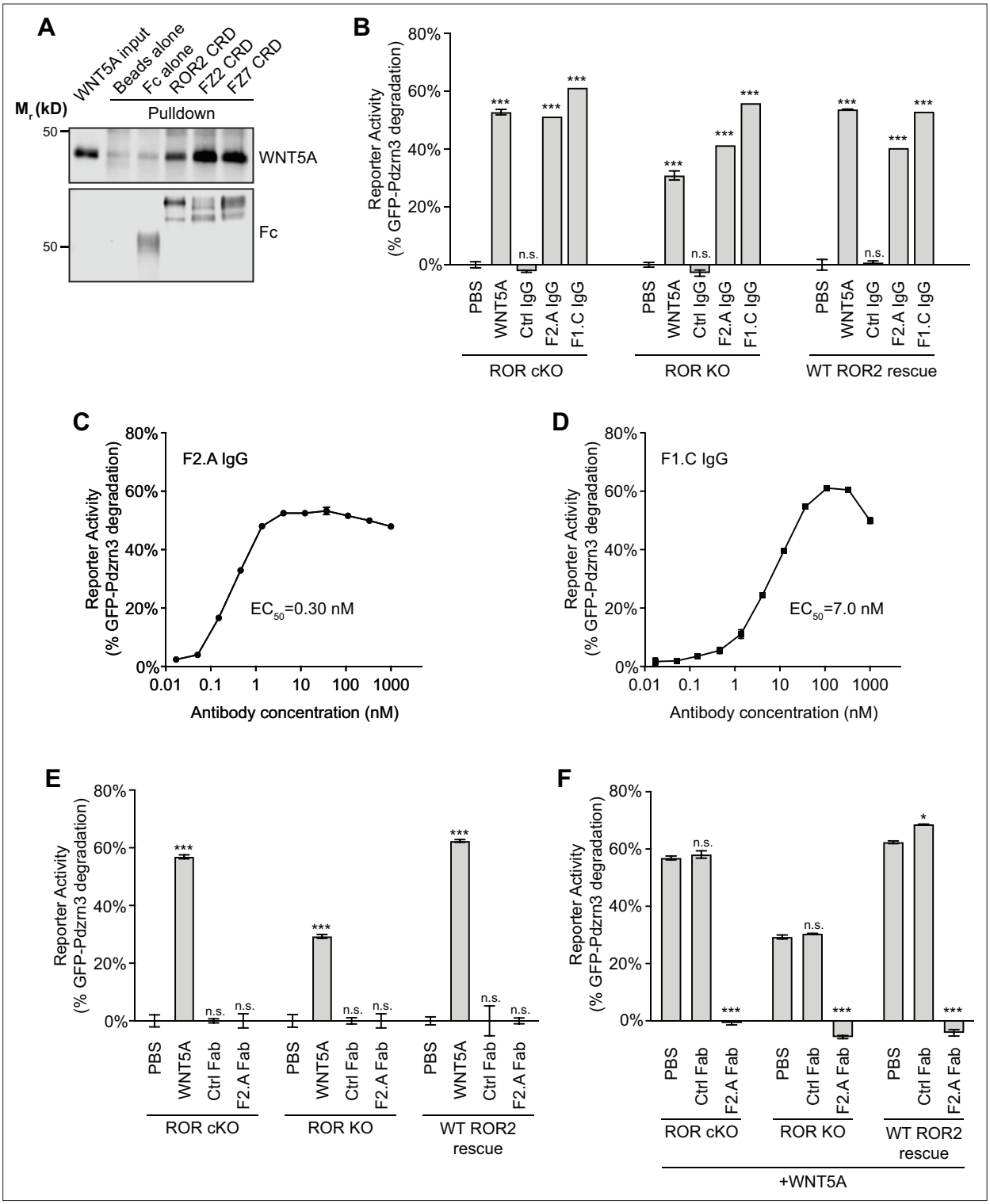

Figure 4. Involvement of Frizzled (FZ) in WNT5A-ROR signaling. (**A**) Fc fusions of the ROR2, FZ2, and FZ7 cysteine-rich domains (CRDs) immobilized on protein A-coated beads were tested for their ability to pull down WNT5A. Protein A beads alone and protein A beads coated with Fc were used as negative controls. 9.3% of the input and 33% of the pulled down materials were analyzed on a 12% SDS-polyacrylamide gel. WNT5A and Fc fusion proteins were detected by western blotting using anti-WNT5A and anti-Flag antibodies (all Fc fusions were tagged with the Flag epitope), respectively. (**B**) Quantification of the effects of the pan-anti-FZ IgG F2.A and anti-FZ1 IgG F1.C in inducing GFP-Pdzrn3 reporter degradation in ROR conditional knockout (cKO) immortalized mouse embryonic fibroblasts (iMEFs), ROR KO iMEFs, and ROR KO iMEFs rescued with wildtype (WT) ROR2. WNT5A was used as the positive control, and an isotype-matching IgG against the Gaussia luciferase was used as the negative control (Ctrl IgG). No IgGs and

Figure 4 continued on next page

Figure 4 continued

WNT5A were mixed in this experiment. All IgGs were used at 200 nM, and WNT5A was used at 200 ng/ml (5.3 nM). WNT5A and FZ IgG stimulations were done in the presence of Wnt-C59 for 6 hr. Each data point was calculated from the median fluorescence ([before antibody treatment – after antibody treatment]/before antibody treatment) of the GFP-Pdzrn3 reporter. Error bars represent ± SEM calculated from three technical replicates; 20,000 cells per replicate. t-Test (unpaired) was performed to determine the statistical significance of each treatment vs. PBS. (**C**) Dose-response analysis showing the ability of the bivalent pan-anti-FZ IgG F2.A to activate WNT5A signaling, as assayed by GFP-Pdzrn3 degradation in ROR KO iMEFs treated with Wnt-C59 but without WNT5A. (**D**) Dose-response analysis showing the ability of the bivalent anti-FZ1 IgG F1.C to activate WNT5A signaling, as assayed by GFP-Pdzrn3 degradation in ROR KO iMEFs treated with Wnt-C59 but without WNT5A. (**E**) Quantification of the effects of the monovalent Fab fragment of the F2.A antibody in inducing GFP-Pdzrn3 degradation in ROR cKO iMEFs, ROR KO iMEFs, and ROR KO iMEFs rescued with WT ROR2. All iMEFs were treated with Wnt-C59. WNT5A was used as the positive control, and an isotype-matching Fab against the Gaussia luciferase was used as the negative control (Ctrl Fab). The Ctrl and F2.A Fabs were used at 200 nM, and WNT5A was used at 200 ng/ml (5.3 nM). No cells were simultaneously treated with Fab and WNT5A in this experiment. Each data point was calculated from the median fluorescence ([before antibody treatment – after antibody treatment]/before antibody treatment) of the GFP-Pdzrn3 reporter. Error bars represent ± SEM calculated from three technical replicates; 20,000 cells per replicate. t-Test (unpaired) was performed to determine statistical significance of each treatment vs. PBS. (**F**) Quantification of the effects of the monovalent Fab fragment of the F2.A antibody in inhibiting WNT5A-induced GFP-Pdzrn3 reporter degradation in ROR cKO iMEFs, ROR KO iMEFs, and ROR KO iMEFs rescued with WT ROR2. All iMEFs were treated with Wnt-C59. An isotype-matching Fab against the Gaussia luciferase was used at the negative control (Ctrl Fab). In all conditions, cells were pretreated with PBS, Ctrl Fab, or F2.A Fab for 30 min and then stimulated with WNT5A in the presence of PBS or Fabs for an additional 6 hr. The Ctrl and F2.A Fabs were used at 200 nM, and WNT5A was used at 200 µg/ml (5.3 nM). Each data point was calculated from the median fluorescence ([before WNT5A treatment – after WNT5A treatment]/before WNT5A treatment) of the GFP-Pdzrn3 reporter. Error bars represent ± SEM calculated from three technical replicates; 20,000 cells per replicate. t-Test (unpaired) was performed to determine statistical significance of each treatment vs. PBS. ***Figure 4—source data 1*** (related to panel B). ***Figure 4—source data 2*** (related to panel C). ***Figure 4—source data 3*** (related to panel D). ***Figure 4—source data 4*** (related to panel E). ***Figure 4—source data 5*** (related to panel F).

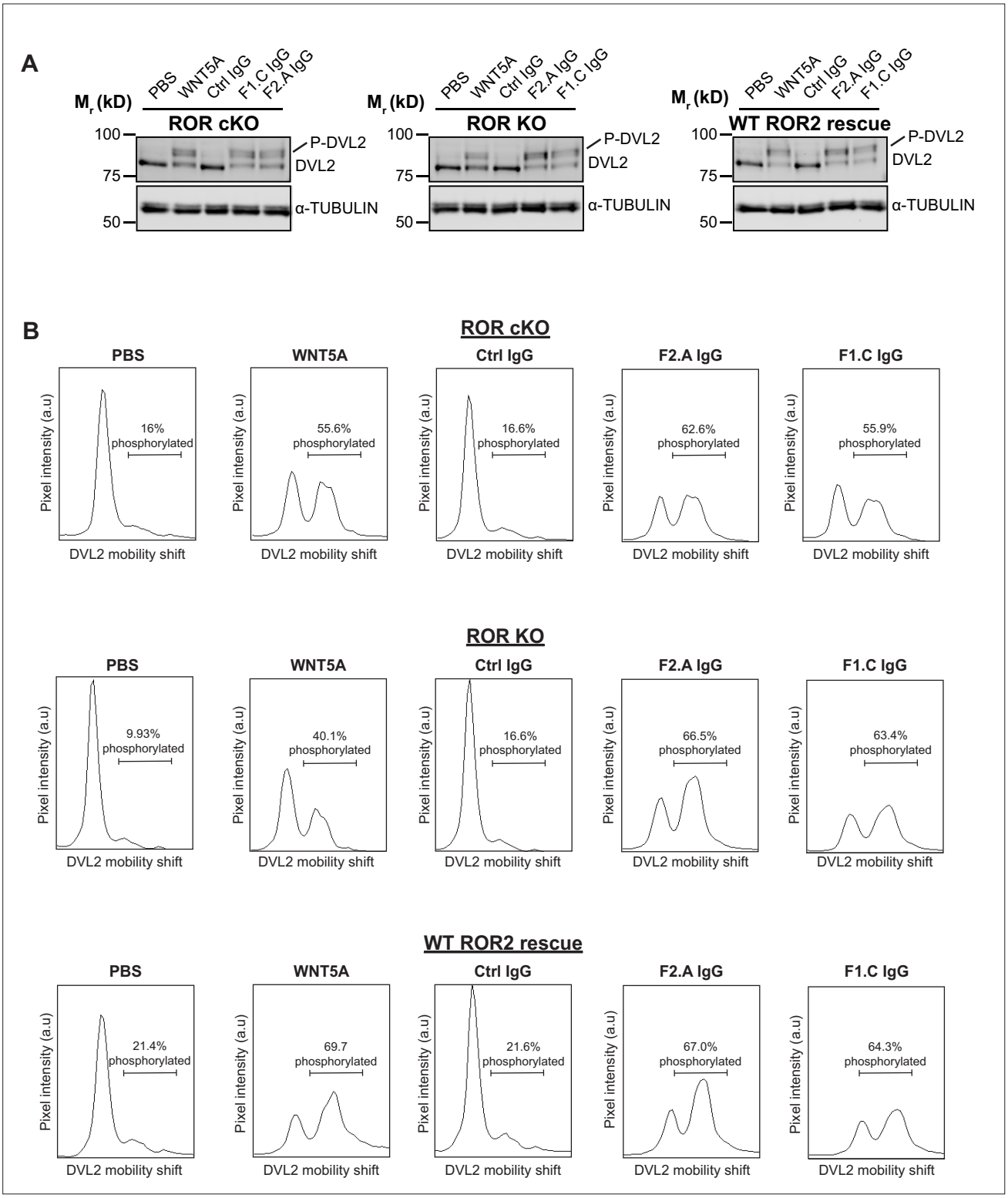

Figure 4—figure supplement 1. Activation of WNT5A signaling by anti-Frizzled (FZ) IgGs, as assayed by Dishevelled 2 (DVL2) phosphorylation. (A) Western blots showing the abilities of F1.C and F2.A IgG to activate WNT5A signaling, as assayed by DVL2 phosphorylation, in ROR conditional knockout (cKO) immortalized mouse embryonic fibroblasts (iMEFs), ROR KO iMEFs, and ROR KO iMEFs rescued with wildtype (WT) ROR2. The Ctrl, F2.A, and F1.C IgGs were used at 200 nM, and WNT5A was used at 100 ng/ml (2.6 nM). Cells were pretreated with Wnt-C59 and maintained in Wnt-C59 during the 6 hr stimulation period. (B) Quantification of DVL2 phosphorylation by densitometry. % phosphorylation is calculated as the portion of total DVL2 signal that is upshifted.

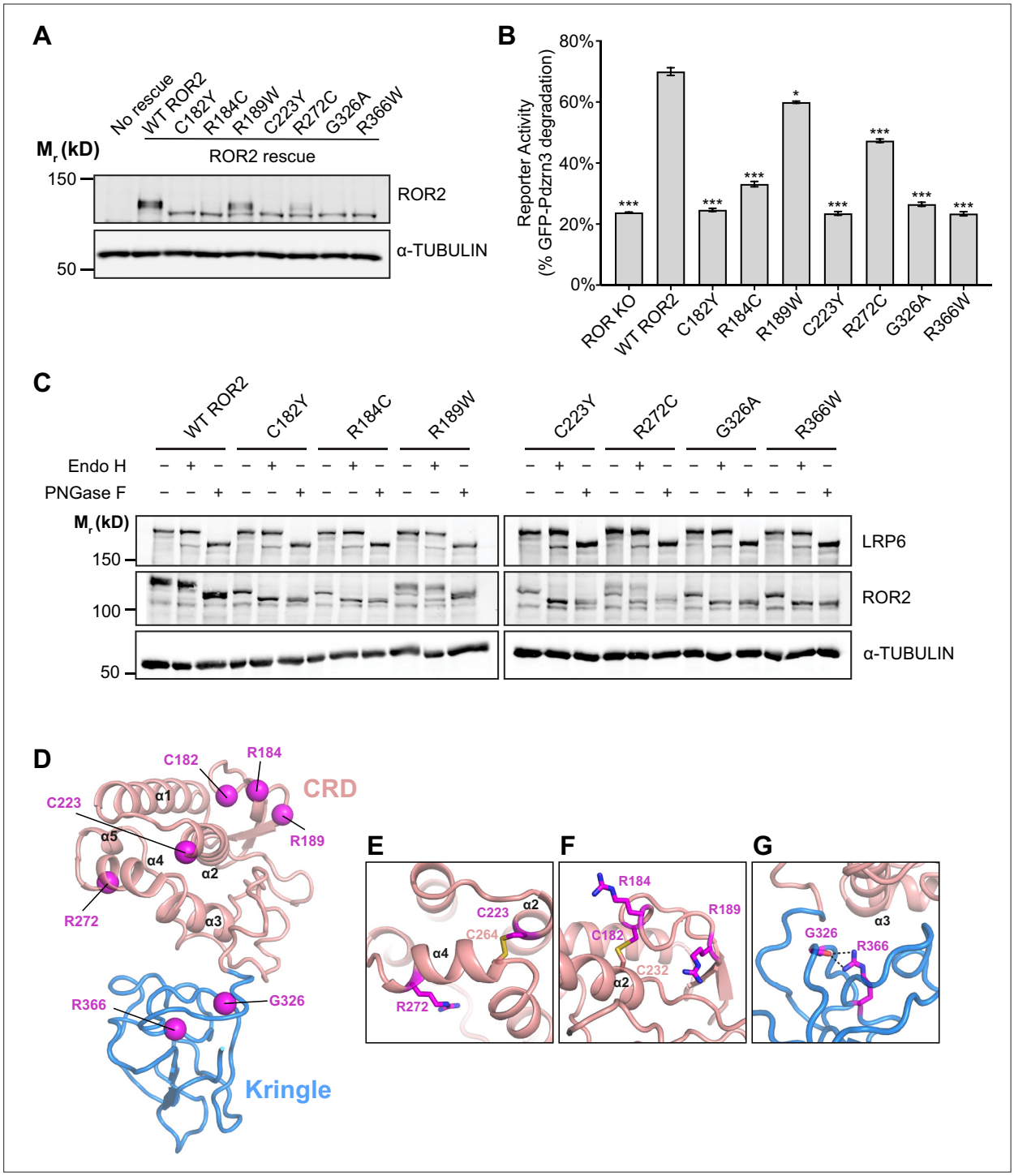

Figure 5. Analysis of Robinow syndrome mutations in the ROR2 cysteine-rich domain (CRD) and Kringle (Kr) domain. (**A**) Western blot showing expression of wildtype (WT) ROR2 and Robinow syndrome ROR2 mutants in the ROR knockout (KO) immortalized mouse embryonic fibroblast (iMEF) reporter cells. (**B**) Quantification of the effects of Robinow syndrome ROR2 mutants in rescuing WNT5A-ROR signaling, as assayed by GFP-Pdzrn3 degradation. Cells were treated with 200 ng/ml (5.3 nM) WNT5A for 6 hr. Error bars represent ± SEM calculated from three technical replicates. t-Test (unpaired) was performed to determine statistical significance for mutants vs. WT ROR2 rescue. (**C**) Western blots showing the sensitivity of WT ROR2 and Robinow syndrome ROR2 mutants to endoglycosidase H (Endo H) and peptide-*N*-glycosidase F (PNGase F). LRP6 was used as a control substrate for Endo H and PNGase F, and α-TUBULIN was used as the loading control. (**D**) Structure of the ROR2 CRD-Kr tandem domains showing the location of the Robinow syndrome mutations. (**E**) Close-up view of C223 and R272. (**F**) Close-up view of C182, R184, and R189. (**G**) Close-up view of G326 and R366.
Figure 5—source data 1 (related to panel B).

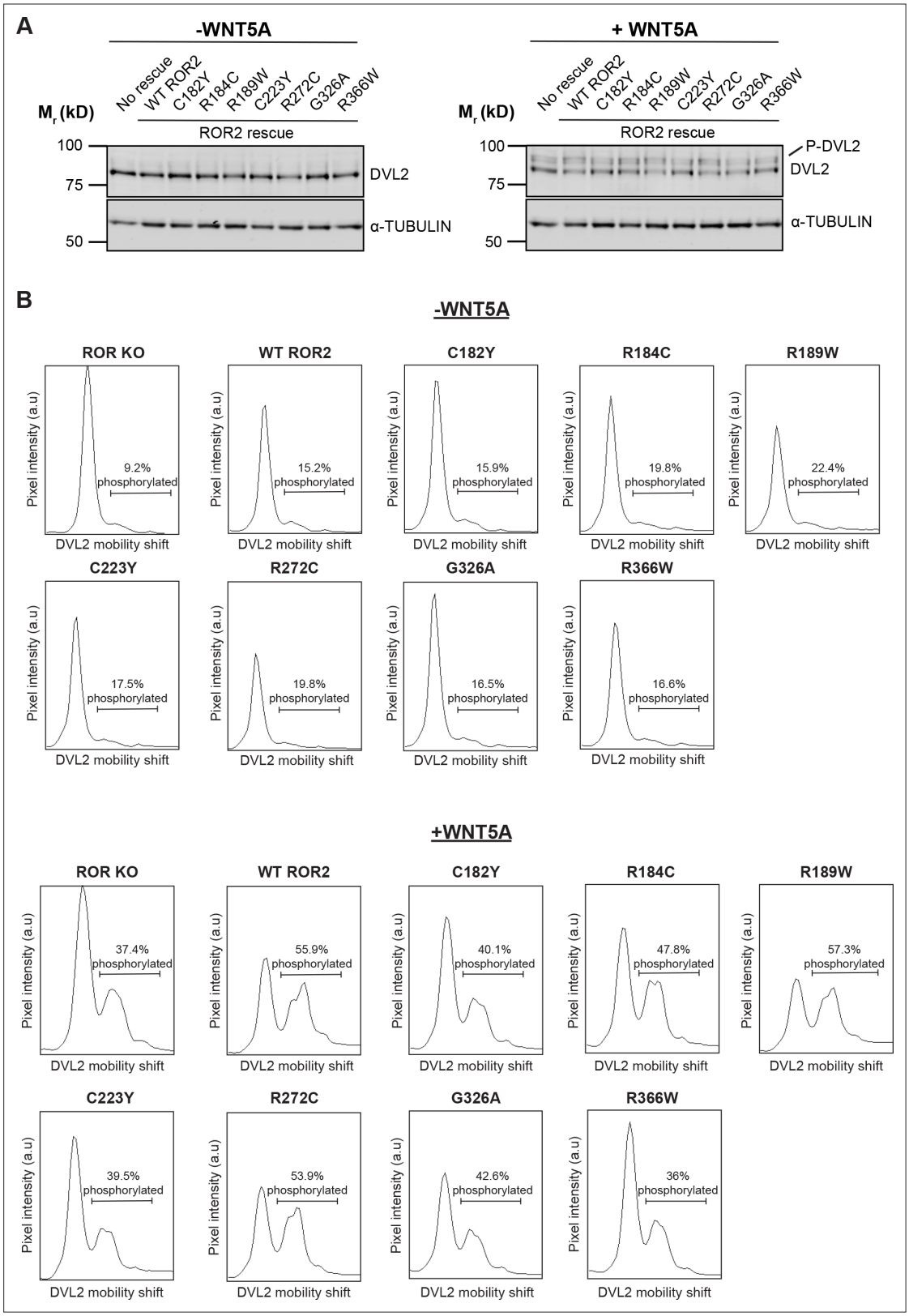

Figure 5—figure supplement 1. Signaling capabilities of Robinow syndrome mutants, as assayed by Dishevelled 2 (DVL2) phosphorylation. (**A**) Western blots showing the abilities of wildtype (WT) ROR2 and Robinow syndrome ROR2 mutants to rescue WNT5A signaling in the ROR knockout (KO) immortalized mouse embryonic fibroblast (iMEF) reporter cells, as assayed by DVL2 phosphorylation. Wnt-C59 pretreated cells were stimulated with WNT5A (100 ng/ml or 2.6 nM) for 6 hr. (**B**) Quantification of DVL2 phosphorylation by densitometry. % phosphorylation is calculated as the portion of total DVL2 signal that is upshifted.

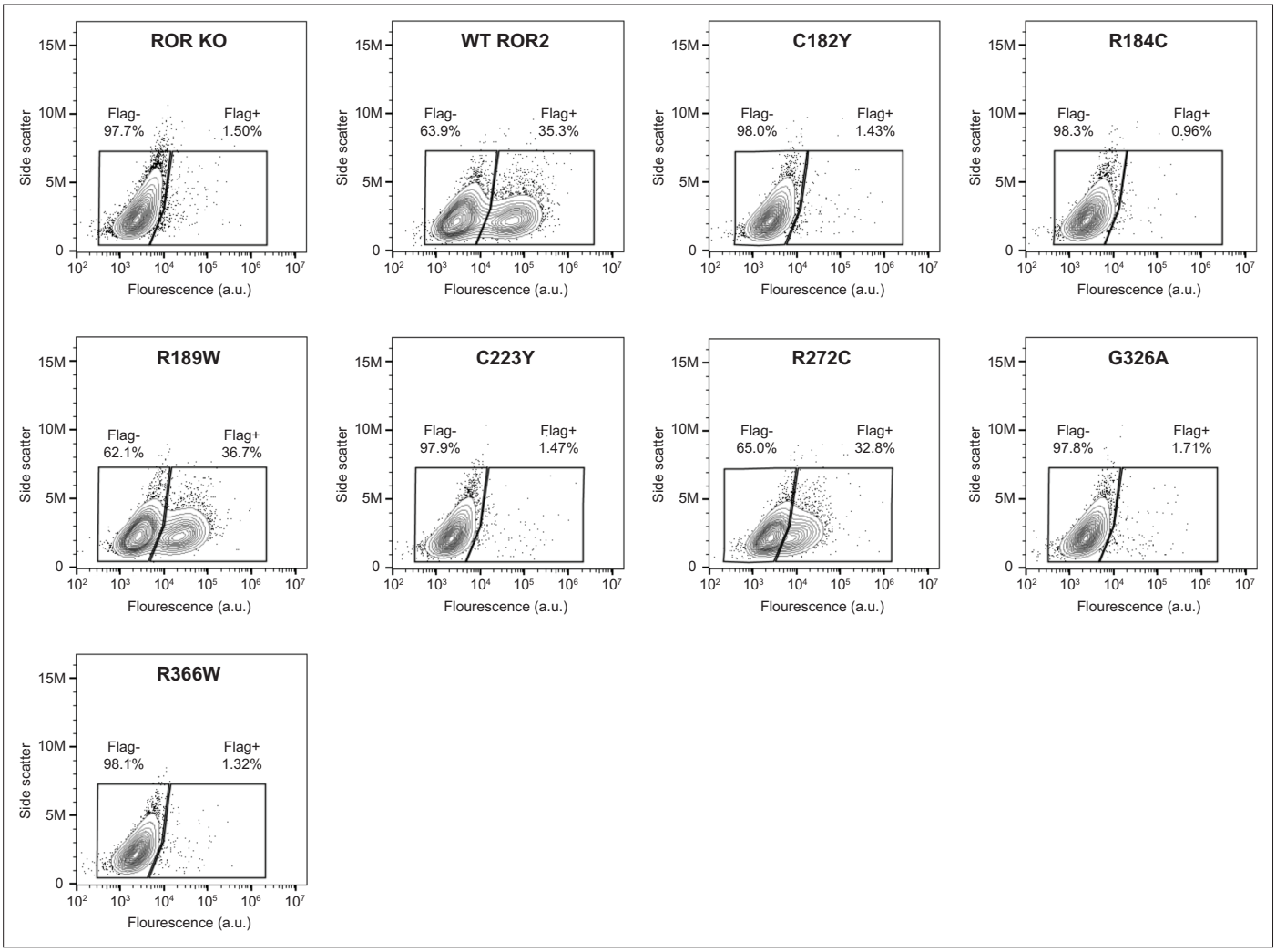

Figure 5—figure supplement 2. Surface expression analysis of Robinow syndrome mutations in the ROR2 cysteine-rich domain (CRD) and Kringle (Kr) domains. Wildtype (WT) ROR2 and Robinow syndrome ROR2 mutants were tagged on the N-terminus with a Flag tag. Anti-Flag immunostaining was performed on live cells to assess the cell surface expression levels of these ROR2 mutants. ROR knockout (KO) cells and ROR KO cells expressing the WT ROR2 rescue construct were used as the negative and positive controls, respectively.

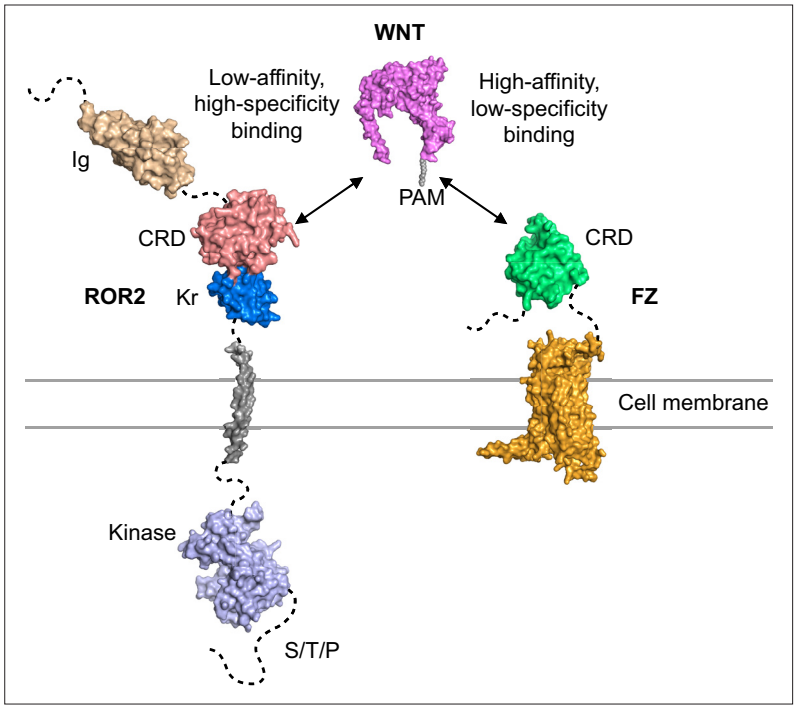

Figure 6. Model of ROR2 cysteine-rich domain (CRD) and Frizzled (FZ) action in WNT5A-ROR signaling.